Evidence of vortex-induced lift on a yawed wing in reverse flow

Vrishank Raghav, Michael Mayo, Rafael Lozano and Narayanan Komerath

Proceedings of the Institution of Mechanical Engineers, Part G: Journal of Aerospace Engineering published online 20 November 2013
DOI: 10.1177/0954410013511597

Technical Note

Institution of MECHANICAL ENGINEERS
Journal of AEROSPACE ENGINEERING

Proc IMechE Part G:
J Aerospace Engineering
0(0) 1–8

DOI: 10.1177/0954410013511597
uk.sagepub.com/jaero
SAGE

Evidence of vortex-induced lift on a yawed wing in reverse flow

Vrishank Raghav, Michael Mayo, Rafael Lozano and Narayanan Komerath

Abstract

Rotating blades on helicopters experience reverse flow under high advance ratio conditions. Here, reverse flow is characterized by the flow traveling from the sharp trailing edge to the blunt leading edge. Uncertainty in the blade aerodynamic loads under these conditions has been a limitation during the design of high-speed rotorcraft. In this work, we hypothesize that the reverse flow over a yawed blade includes phenomena similar to the formation of a leading edge vortex on sharp-edged delta wings. Low-speed wind tunnel experiments are reported on a scaled version of a rotor blade in regular and reverse flow over a large range of yaw and moderate ranges of angle of attack. Force measurements indicate a deviation from yawed-wing expectations at high yaw angles. Surface flow visualization via tufts shows the existence of an attached span-wise vortex on the wing.

Keywords

Reverse flow, vortex lift, yawed wing, high advance ratio, helicopter

Date received: 26 July 2013; accepted: 27 September 2013

Introduction

Most military and civil helicopters operate at low flight Mach numbers ($0.1 < M < 0.2$) primarily because of their aerodynamic limitations. One of the limitations is the behavior of the retreating blade at high advance ratios of $\mu_a \geqslant 0.5$, (see Perry[2]), where advance ratio is defined as the ratio of the forward flight speed to the rotational tip speed of the rotor. Recent developments[3] in high-speed rotorcraft design exceed advance ratios of 0.5. Concepts such as slowed rotors for high-speed rotorcraft (for example, Carter[4]) include the possibility of flying as fast as today's business jets (equivalent to $\mu_a > 1$) and yet benefiting from vertical take-off and landing capability. Under such high advance ratio conditions, a significant portion of the rotor experiences flow from the trailing edge to the leading edge of the rotor blade (referred to as reverse flow, see illustration in Figure 1). This phenomenon has also been observed to occur on horizontal-axis wind turbine blades in yaw. However, there are few studies on rotors at high advance ratios where reverse flow is significant. The earliest full scale investigations include a Pitcairn PCA-2 autogyro rotor,[5] a UH-1D teetering rotor,[6] and an H-34 articulated rotor.[7]

Harris[8] performed correlation studies on full-scale data sets and showed that computational fluid dynamics (CFD) coupled with comprehensive analysis tools failed to adequately predict airloads in the reverse flow region and rotor performance at high advance ratios $\mu_a \geqslant 1.0$. Recent experimental work conducted by Datta et al.[9] on a slowed rotor showed large impulses in pitch-link loads on the retreating blades and evidence of "reverse chord dynamic stall" at advance ratios approaching unity. Comprehensive analysis using CAMRAD II performed by Yeo[10] on the slowed rotor dataset showed fair airload and structural load correlation. Coupled CFD and comprehensive analysis on the UH-60 A dataset performed by Potsdam et al.[11] showed unconventional wake patterns, a lower surface vortex on the retreating blade which was attributed to "reverse chord dynamic stall," and poor prediction of the pitch link loads on the advancing and retreating blades.

The motivation for this work is to better understand the aerodynamic behavior of a *rotating blade* in reverse flow by first understanding the aerodynamic characteristics of a static yawed wing in reverse flow.

Daniel Guggenheim School of Aerospace Engineering, Georgia Institute of Technology, Atlanta, Georgia, USA

Presented at 2012 ASME International Mechanical Engineering Congress & Exposition (Lozano et al.[1])
Corresponding author:
Narayanan Komerath, Daniel Guggenheim School of Aerospace Engineering, Georgia Institute of Technology, Atlanta, GA 30332, USA.
Email: komerath@gatech.edu

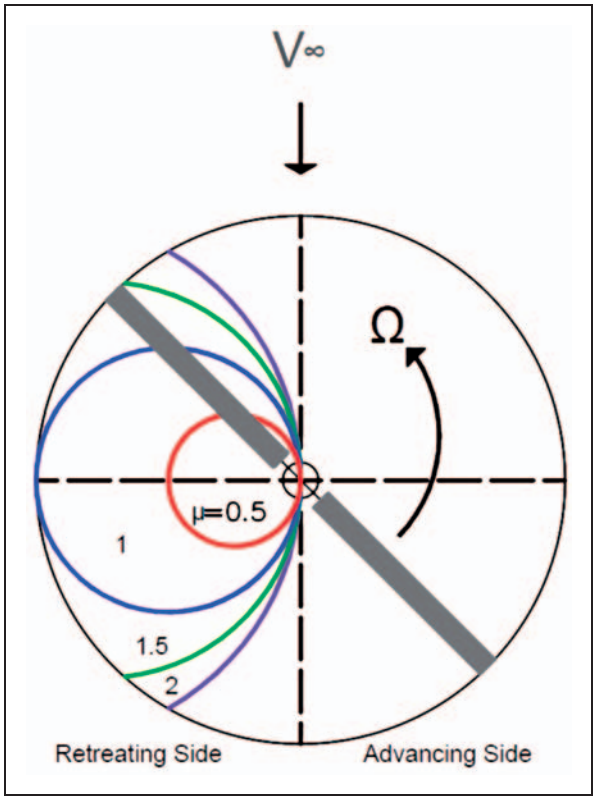

Figure 1. Extent of reverse flow region at various advance ratios (μ_a).

The aerodynamic behavior of a rotating blade is complex which include effects of yaw, aspect ratio, centripetal acceleration, and rotor vortex interaction. A static yawed wing experiment allows for the decoupling of rotational effects from the complex phenomenon present in the reverse flow region. The wing used in this study is from a two-bladed rotor that has been used in past dynamic stall research by Raghav[12] at the John Harper low-speed wind tunnel (test section dimensions of 2.13 m × 2.74 m), and is amenable to be used at high advance ratios to study rotation effects in a later phase of this investigation. Force measurements are reported on a finite wing at various yaw angles in the reverse flow regime. In addition, tuft flow visualization was performed to qualitatively understand the surface flow pattern of yawed wings in reverse flow.

Experimental setup

The experiments were conducted in the John Harper 2.13 m × 2.74 m low-speed wind tunnel at the Georgia Institute of Technology. The closed circuit tunnel is powered by a three-phase 600-hp induction motor controlled by a variable frequency drive. The drive is a closed loop controller with 0.1% error in motor speed setting. The turbulence intensity in the wind tunnel is 0.05% measured at a freestream velocity of 110 ft/s (33.5 m/s). The turbulence intensity reported here is computed using velocity fluctuations data gathered after applying a 1 Hz high-pass filter and a 2.5 kHz low-pass filter.

Table 1. Specifications of the wing used in the experiments.

Description	Value	Units
Span (b)	0.622	meters
Chord (c)	0.178	meters
Aspect ratio (AR)	3.49	
Airfoil	NACA0013	

A finite wing with a NACA 0013 profile (see Table 1 for specifications) was used to conduct the experiments. A drawing and a photo of the setup in the wind tunnel is shown in Figure 2. The wing was mounted onto a two degree of freedom rig allowing the blade to yaw and pitch. The pitch (angle of attack, α) was controlled by a high torque stepper motor reduced with a 30 : 1 gearbox with a resolution of 0.1° in pitch. The yaw angle (ψ) was controlled by a high torque stepper motor which had a resolution of 1°. The stepper motors were controlled by a NI motion controller–nuDrive interfaced to a desktop computer via LABVIEW.

A 6-DOF ATI Delta load-cell transducer interfaced to the computer via LABVIEW was used to measure force and moments on the wing. A three-dimensional rotation matrix was used to keep track of the forces and moments in each coordinate. The tuft flow visualization was performed using 2.5 cm long pieces of yarn taped at 2.5 cm spacing to the suction side of the wing. A high-definition video camera was used to record the visualization.

Flow and test conditions

The tunnel dynamic pressure was measured using a Baratron, differential pressure transducer connected to a pitot-static tube mounted to the ceiling at the upstream end of the test section. Chord Reynolds number (Re) was maintained at a constant by varying the freestream velocity (U_∞) as required depending on the measured temperature and pressure during each experimental run. The data were collected at a sampling rate of 10 kHz (far above the frequency response range of the load cell) and ensemble averaged over 300,000 samples. The various test cases are summarized in Table 2 and described below:

1. The first test was to validate the experimental method for regular flow against published data.
2. The second test explores the effects of yaw angle on the lift curve slope of the wing in reverse flow conditions at two Reynolds numbers. The lift curve slope was determined by measuring the lift through a range of angle of attack as shown in Table 2. Angle of attack resolution was chosen

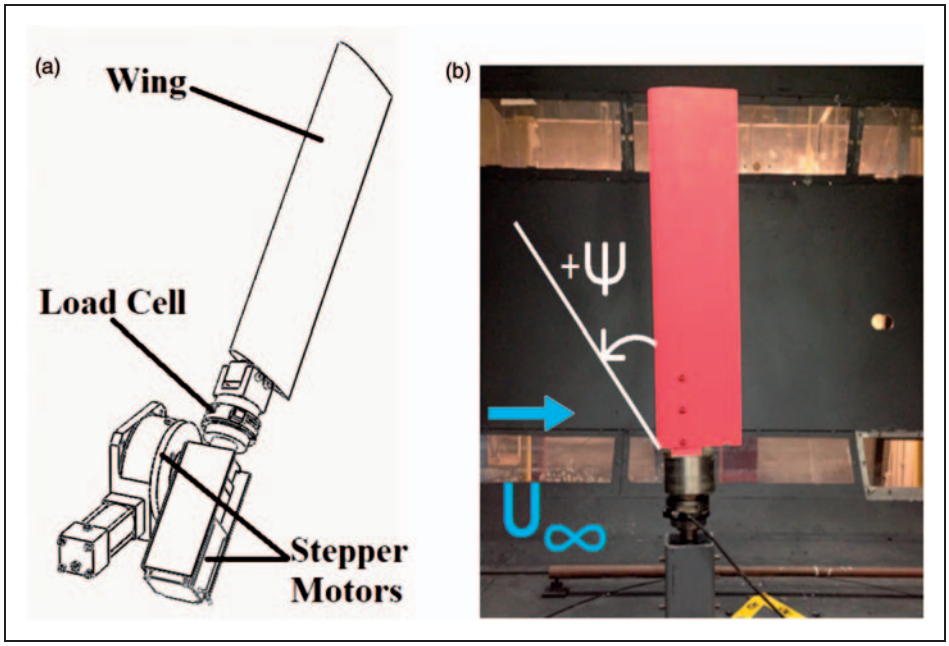

Figure 2. Experimental setup. (a) Drawing of the wing setup. (b) Side view of the rotor setup in the wind tunnel.

Table 2. Test matrix for force measurements.

Test	Flow type	Data acquired	Variable	Re ($\times 10^5$)
1	Regular flow	Validation	$0^\circ \leqslant \alpha \leqslant 30^\circ$	1.7
2	Reverse flow	Lift curve	$180^\circ \leqslant \alpha \leqslant 200^\circ$ $0^\circ \leqslant \psi \leqslant 60^\circ$	1.7 and 3.0
3	Reverse flow	Flow visualization	$180^\circ \leqslant \alpha \leqslant 210^\circ$ $\psi = 30^\circ, 45^\circ$	1.7 and 3.0

appropriately to match the region of the lift curve being measured (lower resolution in the linear region and higher resolution near the stall region). The lift curve slope was determined over a range of yaw angles in increments of 5°.

3. The third test was tuft flow visualization at two Reynolds numbers and two yaw angles. In this case, the wing was pitched through the angle of attack range in increments of 5°.

Uncertainty estimates

The total error in measurement of coefficient of lift, drag, and pitching moment was computed to be ±1.61% in the worst case. The total error was computed using the individual errors of the parameters listed in Table 3. The ensemble averaged data are very repeatable with minimal scatter at each measured point, as observed in the results and discussion section. In addition, a detailed error analysis of the wing geometry was performed. The average error of thickness and chord length when compared to the standard NACA 0013 was around 1.0% of each dimension, with the root mean square error less than 0.1%.

Table 3. Summary of errors.

Parameter	Range considered	Uncertainty
Freestream velocity	$0 - 30$ m/s	±0.33%
Reynolds number	$1.7 \times 10^5 - 3 \times 10^5$	±1000
Load-cell calibration	0–15 N	±1.37%
Yaw and pitch angle	$0^\circ - 60^\circ$	±0.05°

Results and discussion

As mentioned earlier, the validation was first performed by measuring lift, drag, and pitching moment at a Reynolds number of 1.7×10^5 and angle of attack range of $0^\circ \leqslant \alpha \leqslant 30^\circ$. Figure 3(a) illustrates the validation data for the wing between $0^\circ \leqslant \alpha \leqslant 20^\circ$. The slope of the linear portion of the lift curve was determined to be 0.0692/deg = 3.956/rad using a linear fit. This was compared with previously published data by Jacobs[13] for a two-dimensional airfoil (infinite wing) at a similar Reynolds number (1.7×10^5). Since the published data were for a two-dimensional airfoil, it was corrected for aspect ratio using the following equation:

$$C_{L_\alpha} = \frac{c_{l_\alpha}}{1 + \frac{57.3 c_{l_\alpha}}{\pi e AR}} \quad (1)$$

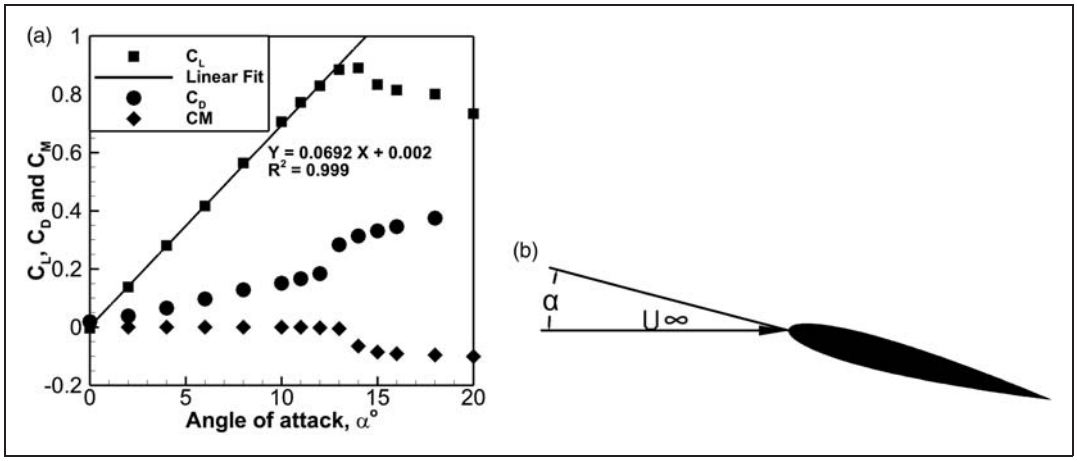

Figure 3. Regular flow at $Re = 1.7 \times 10^5$. (a) Lift, drag, and pitching moment. (b) Wing orientation.

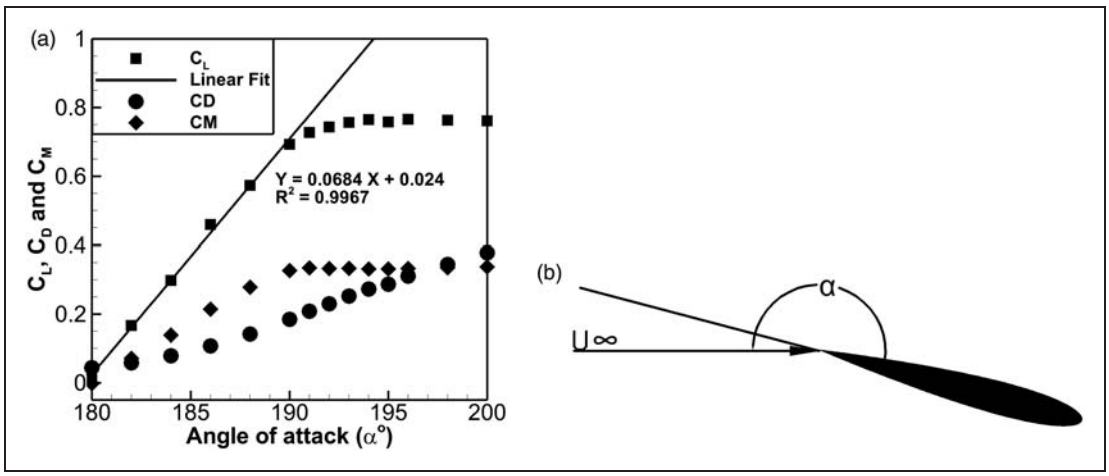

Figure 4. Regular flow at $Re = 1.7 \times 10^5$. (a) Lift, drag, and pitching moment. (b) Wing orientation.

where C_{L_α} is the lift curve slope corrected for aspect ratio, c_{l_α} is the lift curve slope of an infinite wing, e is Oswald's efficiency factor, and AR is the aspect ratio of the wing.

The published lift curve for the infinite wing at $Re = 1.7 \times 10^5$ was 6.03/rad, which was corrected for aspect ratio and determined to be 3.75/rad. This is a close match to the lift curve slope obtained in these experiments considering the following: (a) the corrections are accurate only for aspect ratio greater than 4.0 (while in these experiments aspect ratio of the wing is 3.5), (b) the wing model used in this experiment has a rotor mount on one end which weakens the tip vortex at the blade root, causing a higher lift curve slope, and (c) the mount interference with the lift force is not quantified at the writing of this technical note.

Lift force in reverse flow

Aerodynamic loads on the wing in reverse flow at $\psi = 0$ were measured; this is essentially the equivalent of a wing at a conventional angle of attack of 180°. Figure 4(a) illustrates the lift, drag, and pitching moment of the wing in reverse flow. Here, the lift curve slope (0.0684/deg = 3.92/rad) was slightly lower than that of a wing in regular flow. This lift curve slope is fairly similar to the aspect ratio corrected lift curve slope of 3.5/rad found by Critzos et al.[14] for reverse flow on a NACA 0012 airfoil tested at $Re = 5 \times 10^5$. An interesting observation is the linear increase of pitching moment with lift, which indicates that the center of pressure is no more located at the quarter chord (0.25 c) of the wing with respect to the blunt leading edge. Instead, the data suggested that the center of pressure in reverse flow varies between 0.76 c and 0.82 c with respect to the blunt leading edge.

The lift curve plots at various yaw angles in reverse flow are illustrated in Figure 5. The following are the observed salient features of the wing in reverse flow:

1. As expected, the lift curve slope decreases with increasing yaw angle and the stall angle increases with increasing yaw angle.

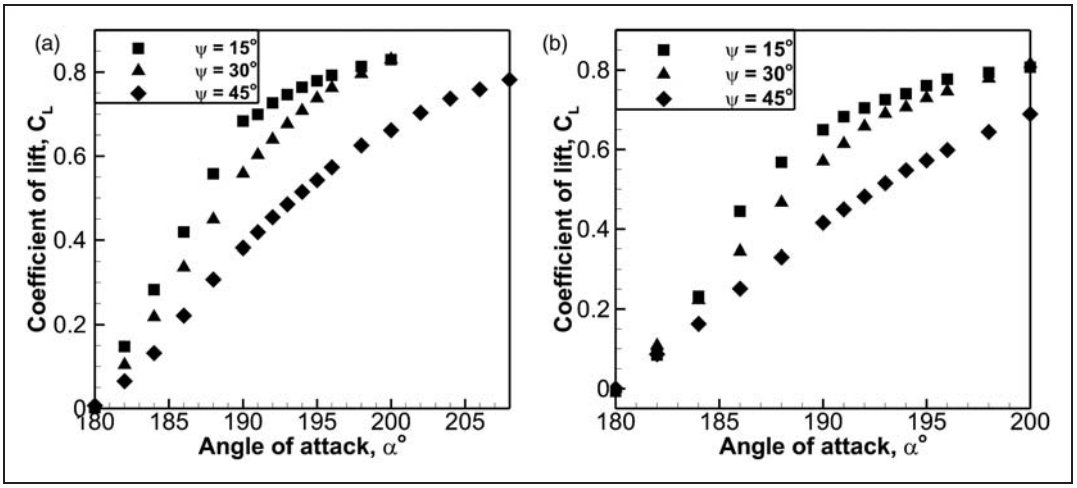

Figure 5. Lift curves at varying yaw angles of the wing in reverse flow: (a) $Re = 1.7 \times 10^5$ and (b) $Re = 3.0 \times 10^5$.

2. At yaw angle $\psi \geqslant 15^\circ$, the lift curves are observed to undergo a "soft-stall." In other words, there is no linear increase of lift with angle of attack. Instead is a small increase in lift with angle of attack. The physical reasoning for this trend could be explained by the behavior of the surface flow described in the next section.

A summary of lift curve slopes in regular flow and in reverse flow is illustrated in Figure 6. These plots are composed of multiple experiments with each data point showing the lift curve slope at each yaw angle.

1. The lift curve slope in regular flow exhibits the expected variation with yaw angle ($cos^2\psi$).
2. In reverse flow at $Re = 1.7 \times 10^5$, the lift curve slope starts out higher than the expected $cos^2\psi$ variation and maintains that behavior at higher yaw angles ($\psi \leqslant 50^\circ$). In addition, at $Re = 3.0 \times 10^5$, the lift curve slopes at high yaw angles are also higher than the expected $cos^2\psi$ fit and the corresponding lift curve slope at $Re = 1.7 \times 10^5$. The slight increase in lift curve slope could be an effect of Reynolds number; however, the limited range of Reynolds number does not allow for a complete interpretation of the effect of Reynolds number. This could suggest that there is an extra source of lift in the reverse flow regime at high yaw angles, most likely the initiation of vortex-induced lift at high yaw angles.

Surface flow visualization in reverse flow

In order to further investigate the high lift curve slopes in reverse flow when compared to regular flow, tuft flow visualization was performed. The visualization was used to observe the nature of surface flow patterns on the yawed wing and to reconcile the lift force measurements in reverse flow. The flow

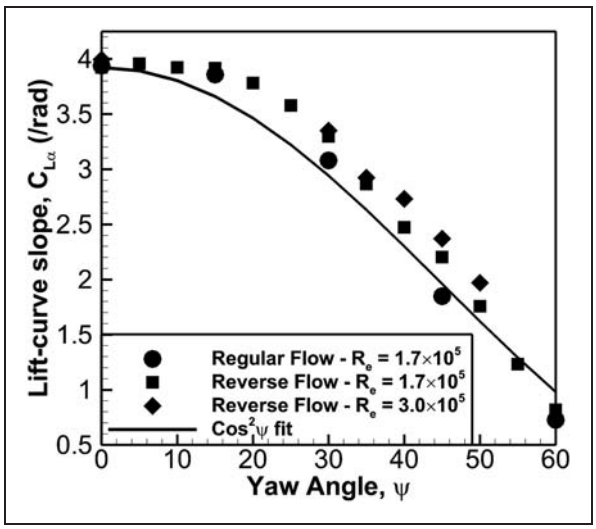

Figure 6. Variation of lift curve slope with yaw angle of the wing in reverse flow.

visualization experiments were conducted at the test conditions indicated in Table 2 and only one test case for flow visualization is presented ($\psi = 45^\circ$ and $Re = 1.7 \times 10^5$). The data also show signs of mount interference, which must be accounted for when drawing any conclusions. However, these are realities to be faced when trying to perform direct comparisons of a blade used in both fixed wing and rotorcraft applications. The variation of surface flow patterns with increasing angle of attack at a Reynolds number $Re = 1.7 \times 10^5$ and Yaw angle $\psi = 45^\circ$ is shown in Figure 7. Please refer to the supplementary video submission for a clear illustration of the flow behavior. In summary:

1. At $\alpha = 185^\circ$, the flow is attached on all sections of the wing and primarily in the freestream direction. A few tufts at the sharp trailing edge are moving in a clockwise, conical rotation pattern when looking from upstream. These could indicate the initiation of an attached vortex.

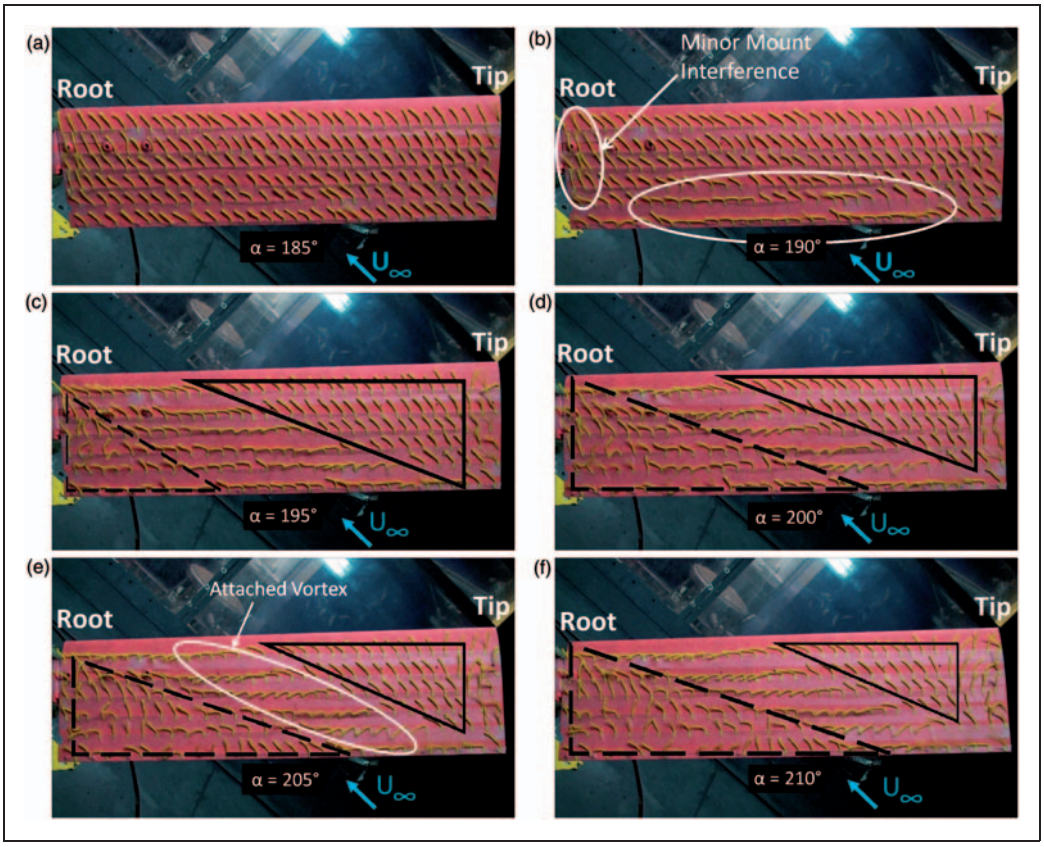

Figure 7. Flow visualization at $\psi = 45^\circ$ and $Re = 1.7 \times 10^5$ in reverse flow. (a) $\alpha = 185^\circ$, (b) $\alpha = 190^\circ$; (c) $\alpha = 195^\circ$; (d) $\alpha = 200^\circ$; (e) $\alpha = 205^\circ$; (f) $\alpha = 210^\circ$.

2. At $\alpha = 190^\circ$, the flow is still attached on all sections of the wing. However, the flow at the sharp trailing edge is predominantly in the span-wise direction showing signs of vortex growth (indicated with an oval in Figure 7(b)). The tufts aligned in the span-wise direction exhibit violent conical motions corresponding to the growth of an attached span-wise vortex.
3. At $\alpha = 195^\circ$, the surface flow exhibits three distinct flow patterns:
   (a) The surface flow is still attached on most parts of the wing, and this is depicted with a solid triangle.
   (b) A significant portion of the surface flow is in the span-wise direction, signifying the expansion of an attached vortex.
   (c) The tufts in a small section of the wing near the root exhibit random chaotic motion suggesting flow separation (marked by a dashed triangle). As the flow reaches the root of the yawed wing, it experiences an adverse pressure gradient due to a drop in span-wise velocity. This adverse pressure gradient results in flow separation and appears to cause vortex bursting as it would on a delta wing (Kohlman[15] and Payne[16]).
4. At $\alpha \geqslant 200^\circ$, the surface flow does not show any significant changes. However, now a clear demarcation is seen between attached and separated flow regions indicated by solid and dashed triangles, respectively. Clearly as angle of attack increases, the separated region is increasing in size and the attached region is decreasing in size, while the attached vortex flow maintains its size.
5. At this point, it is also important to mention that the interference of the mount in a small aspect ratio wing (as in this case) would be significantly higher when compared to a larger aspect ratio wing. On a larger aspect ratio wing, the separated flow near the root of the wing would be *expected* to be a smaller proportion of the total blade area.

The flow visualization observations can now used to reconcile the behavior of lift at high yaw angles $\psi \geqslant 20^\circ$. As observed in Figure 5, there is no post-stall drop in lift. This could be directly linked to the existence of an attached vortex on the yawed wing surface in reverse flow. In addition, the small regions of attached flow also help in producing lift. However, as one of the reviewers of this paper pointed out, it is important to note that the surface flow patterns are specifically for a yawed wing which would be different than a swept wing.

Based on the flow visualization experiments, the surface flow topology on a yawed wing in reverse flow is sketched in Figure 8. The flow topology

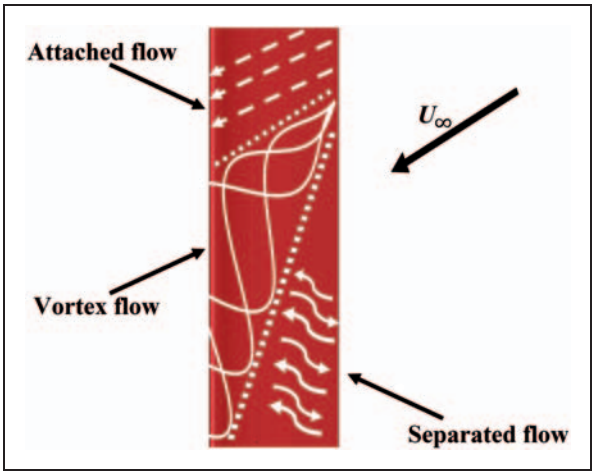

Figure 8. Proposed surface flow topology over a yawed wing in reverse flow.

shows the three distinct flow regimes—attached flow, vortex flow, and separated flow demarcated by the dotted lines. It is worth noting that the position and shape of the attached span-wise vortex closely resembles that of the lower surface vortex predicted by Potsdam et al. (see Figure 25 in Ref. 11), which was attributed to "reverse-chord dynamic stall." The similar vortex observed in this investigation on a static yawed wing could suggest that the vortex predicted by Potsdam et al. may not be an artifact of rotation.

Concluding remarks

The motivation for this work was to better understand the aerodynamic behavior of a rotating blade in reverse flow by first understanding the aerodynamic characteristics of a static wing in reverse flow. Lift forces on a finite wing in regular flow were measured and validated against published data. The same finite wing was then tested in reverse flow regimes at various yaw angles in order to understand the fundamental differences in behavior of the lift characteristics when compared to that in regular flow.

The findings in this work are summarized as follows:

1. The lift behavior of the wing in reverse flow at yaw angles $\psi > 20^\circ$ indicates no post-stall drop in lift.
2. The lift curve slopes in reverse flow were observed to be higher than the corresponding regular flow lift curve slopes at yaw angles $\psi > 20^\circ$. It was also observed that the lift curve slopes at higher yaw angles displayed a small increase with Reynolds number.
3. The above two conclusions suggest that there is an extra source of lift in the reverse flow regime at high yaw angles ($20^\circ \leqslant \psi \leqslant 50^\circ$), indicating the possible initiation of vortex-induced lift at these yaw angles.
4. Surface flow visualization at $Re = 1.7 \times 10^5$ and $\psi = 45^\circ$ confirmed the existence of an attached vortex on the wing in reverse flow. The flow visualization also established the sequence of the development of surface flow patterns on the wing.
   (a) At lower angles of attack ($180 \leqslant \alpha \leqslant 190^\circ$), the surface flow was mostly attached. The flow at the sharp trailing edge was predominantly in the span-wise direction. The tufts aligned in the span-wise direction exhibited violent conical motions showing signs of an incipient and expanding span-wise vortex.
   (b) At higher angles of attack ($\alpha \geqslant 195^\circ$) the surface flow developed three distinct flow regimes—the attached flow, vortex flow, and separated flow.
   (c) The flow separation occurs due to the adverse pressure gradient induced by the mount at the root and appears to cause vortex bursting as it would on a delta wing.
   (d) The area of the separated flow near the mount is *expected* to decrease for a larger aspect ratio wing since the mount induced adverse pressure gradient would be significantly lower.
5. The higher lift curve slopes in reverse flow and the lack of a post-stall drop in lift at high yaw angles is reconciled by the existence of the attached vortex and small regions of attached flow.

Conflict of interest

The authors declare no conflict of interests.

Funding

This work was funded by the Army Research Office (ARO), grant number W911NF1010398.

References

1. Lozano R, Raghav V and Komerath N. Aerodynamics of a yawed blade in reverse flow. In: *Proceedings of ASME 2012 international mechanical engineering congress & exposition*, Houston, Texas, 9–15 November 2012.
2. Perry F. Aerodynamics of the helicopter world speed record. In: *The American Helicopter Society 43rd annual forum proceedings*. Alexandria, VA: American Helicopter Society, 1987, pp.3–15.
3. Walsh D, Weiner S, Arifian K, et al. High airspeed testing of the Sikorsky X2 Technology™ Demonstrator. In: *The American Helicopter Society 67th annual forum proceedings*. Alexandria, VA: American Helicopter Society, 2011.
4. Carter JW, et al. *Extreme mu rotor*. US Patent 6,986,642, USA, 2006.
5. Wheatley JB and Hood MJ. *Full-scale wind-tunnel tests of a PCA-2 Autogiro Rotor*. NACA TR 515, 1935.
6. Charles BD and Tanner WH. *Wind tunnel investigation of semirigid full-scale rotors operating at high advance ratios*. United States Army Aviation Material Laboratories TR 69-2, 1969.

7. MacCloud JL, Biggers JC and Stroub RH. An investigation of full-scale helicopter rotors at high advance ratios and advancing tip Mach numbers. NASA TN D-4632, 1968.
8. Harris FD. *Rotor performance at high advance ratio: theory versus test*. NASA CR 215370, 2008.
9. Datta A, Yeo H and Norman TR. Experimental investigation and fundamental understanding of a full-scale slowed rotor at high advance ratios. *J Am Helicopter Soc* 2013; 58: 1–17.
10. Yeo H. Investigation of UH-60A rotor performance and loads at high advance ratios. *JAircraft* 2012; 50: 576–589.
11. Potsdam M, Datta A and Jayaraman B. Computational investigation and fundamental understanding of a slowed UH-60A rotor at high advance ratios. In: *The American Helicopter Society 68th annual forum*, Fort Worth, Texas, 1–3 May 2012.
12. Raghav V and Komerath N. An exploration of radial flow on a rotating blade in retreating blade stall. *JAm Helicopter Soc* 2013; 58: 1–10.
13. Jacobs EN and Sherman A. *Airfoil section characteristics as affected by variations of the Reynolds number*. NACA TR 586, 1937.
14. Critzos CC, Heyson HH and Boswinkle Jr RW. *Aerodynamic characteristics of NACA 0012 airfoil section at angles of attack from 0 deg to 180 deg*. NACA TN 3361, 1955.
15. Kohlman D and Wentz W. Vortex breakdown on slender sharp-edged wings. *J Aircraft* 1971; 8: 156–161.
16. Payne FM. *Structure of leading-edge vortex flows including vortex breakdown*. PhD dissertation, University of Notre Dame, 1987.